Magnetically bound nature of a holon-doublon pair in two-dimensional photoexcited Mott insulators

K. Iwano and H. Okamoto

Phys. Rev. B **106**, 075128 — Published 15 August 2022

DOI: 10.1103/PhysRevB.106.075128

Magnetically bound nature of a holon-doublon pair in two-dimensional photoexcited Mott insulators

K. Iwano
Graduate University for Advanced Studies, Institute of Materials Structure Science, High Energy Accelerator Research Organization (KEK), 1-1 Oho, Tsukuba 305-0801, Japan

H. Okamoto
Department of Advanced Materials Science, University of Tokyo, Chiba 277-8561, Japan

(Dated: June 9, 2022)

We revisit the holon-doublon binding problem in two-dimensional (2D) photoexcited Mott insulators. Low-energy photoexcited states in Mott insulators are described as a pair state of a doublon and a holon. The most basic question is whether its bound state is formed in the lowest-energy state, and negative and positive responses have been discussed in the past. In this study, we begin with the 2D Hubbard model, and transform it into the first effective model, which is based on the t/U expansion, with U and t being the Hubbard U and the electron hopping energy, respectively, We find that quantitative reliability is assured for $U \gtrsim 10t$. Furthermore, we transform it into a second effective model that selects essential states in the low-energy region. In both the effective models, we distinguish two magnetic terms, namely, the spin-exchange interaction and the three-site transfer, and parametrize the two terms with the parameters, $J_{\rm ex}$ and $J_{\rm 3site}$. By changing the parameters apart from the restriction given by the Hubbard model, any positive $J_{\rm ex}$ value with $J_{\rm 3site} = 0$ yields a finite amount of binding, whereas a finite value of $J_{\rm 3site}$ suppresses the binding significantly, still leaving the Hubbard case of U=10t in the vicinity of the bound-unbound boundary.

I. INTRODUCTION

The physics of two-dimensional (2D) Mott insulators has attracted particular attention since the discovery of the high-T_c superconductivity in the copper oxides [1, 2]. In an ordinary scenario, doped carriers suppress the antiferromagnetic (AF) spin order existing in the undoped systems, leading to metallic or superconducting states beyond a certain critical doping amount. In such cases, we have carriers that correspond to empty sites or doubly occupied sites when we confine our argument to the so-called single-band model, and we usually call them doublons (Ds) and holons (Hs), respectively. Properties and behaviors of such carriers have been discussed intensively, particularly from the viewpoint of magnetic interactions between the carriers and underlying spins [3–7].

In this article, we discuss a similar problem in the context of the photoexcited states. In such states, we naturally expect photoexcited DH pairs. In one dimension, it is well known that they behave as a free DH pair in the whole region of the U/t value, where U and t are the on-site Coulombic energy and the nearest-neighbor (n. n.) hopping energy, respectively, of the 1D Hubbard model [8–13]. We emphasize that the formation of a bound state between such carriers needs the inclusion of the Coulombic attraction working between them at different sites, most typically the n. n. sites (so-called V in the extended Hubbard model). In contrast, the binding or non-binding of a single DH pair is non-trivial in 2D systems. In the 2D Hubbard model, the DH pair on the n. n. sites raises the total energy by U+3.5$J_{\rm ex}$, in the lowest energy state. Here, J_{ex} is the spin-exchange energy and the energy is defined as the site-diagonal energy measured from that of the perfectly ordered AF ground state. Note that $J_{\rm ex}$ is $4t^2/U$ in the strong U limit. The part of 3.5$J_{\rm ex}$ corresponds to the magnetic energy originating from the number of mismatches in the spin alignment. On the other hand, pairs apart from each other have an energy cost of U+4$J_{\rm ex}$. This energy difference is the sole source of the DH binding, while quantum fluctuations are still neglected, thus leaving a question of whether this attraction really stabilizes a DH bound state. Numerous theoretical studies have been performed to understand the optical conductivity of the 2D Hubbard model [14–19]. These studies indicate a peak or enhanced structure at the lower edge of the optical conductivity, although its nature has not been intensively discussed. Recently, a time-dependent density-matrix renormalization group (tDMRG) method is applied to the same Hamiltonian and supports the binding nature of the pair, although a bound state itself is not identified [20].

To illuminate this long-standing problem, we first employ a previously proposed effective model (hereafter, effective model I) [21–25] and calculate the optical conductivity in a 32-site system that is not only larger than the previous one but also has an advantage for a reason later mentioned. For this system size, the aforementioned peak structure is clearly reproduced. However, it is puzzling that even in the presence of such a structure, a clear signature of the DH binding in a real space cannot be confirmed, leaving the possibility that the system size is still insufficient. Hence, we propose an effective model (effective model II) that extracts certain states that are essential to the structure at the lower band edge and thoroughly discuss the binding problem in a sufficiently large system.

II. EFFECTIVE MODEL I AND THE RESULTS BASED ON IT

First, we mention the effective model I, which is derived from the ordinary 2D Hubbard model using a t/U expansion, as presented in Appendix A. It is characterized by three parameters: t, J_{ex}, and $J_{3\mathrm{site}}$, which are illustrated in Fig. 1. Here, t is the same as that in the original Hubbard model, but now implies the direct transfer of a doublon or a holon without changing the energy on the scale of U. The remaining two parameters characterize the magnetic interactions. More explicitly, J_{ex} is the parameter for the spin-exchange interaction, whereas $J_{3\mathrm{site}}$ is for the spin-dependent transfer of a doublon or a hole. Note that J_{ex}=$J_{3\mathrm{site}}$$\simeq 4t^2/U$ in the Hubbard model.

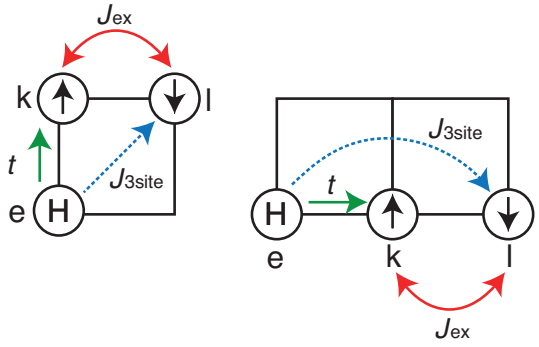

FIG. 1. Illustrations of the interactions included in the effective model I. The case of a holon is presented as an example. The two-way arrow, the solid one-way arrow, and the dashed one-way arrow represent the spin-exchange interactions, the direct transfer, and the three-site term, respectively. Site e is an empty site, and the k and l sites are singly occupied sites.

The effective hamiltonian I thus derived is solved as follows: We determine the ground state and low-lying excited states by exact diagonalization based on the Lanczos method [26]. The whole optical conductivity spectrum is obtained by the continued fraction [27] applied to the ground state. The low-energy part of the spectrum is also determined based on the results from the Lanczos method and is used for a check of the reliability of the spectrum found by the continued fraction.

Because the reliability of this effective model has not been discussed quantitatively thus far, we confirm it using a cluster of 18 sites, as shown in Fig. 2(a), which allows for an exact calculation in the Hubbard model. As is observed in Fig. 2(b), the two optical conductivities are in good agreement for U/t=15 and U/t=20, whereas those for U/t=10 show some disagreement. As the actual copper oxides correspond roughly to U/t=10 [28], this case is the most important in relation to such materials. The results in this case show that the lowest energy peak is well reproduced, suggesting that the effective model can be used in the interpretation of the actual materials.

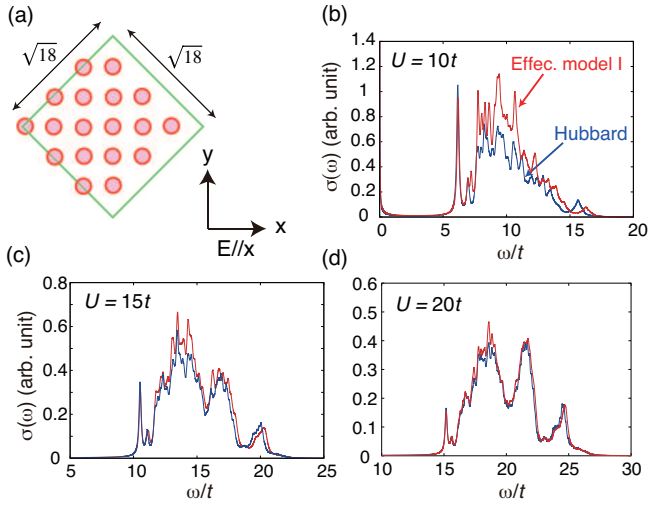

FIG. 2. (a) Cluster of 18 sites and (b) optical conductivities calculated using the Hubbard model and the effective model I. The broadening factor is commonly $0.1t$.

Next, we apply this model to the cluster of 32 sites. In Fig. 3(a), we show the cluster for calculating N=32. In (b), we compare the results for the optical conductivity from the present effective model I and the tDMRG calculation based on the Hubbard model [20]. In the upper panel, the cluster size in the latter case is 8×4, whereas it is 6×6 in the lower panel. Note that in the upper panel, the cluster shapes are different between the two calculations. Although there is some discrepancy, which might arise from the different boundary conditions, the overall coincidence is satisfactory.

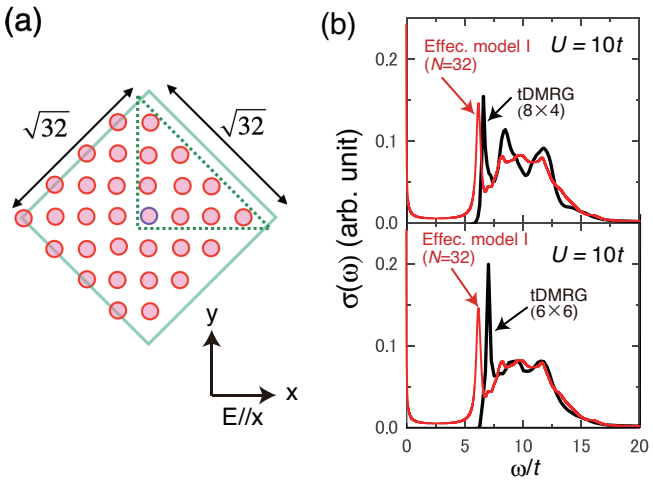

FIG. 3. (a) Cluster used in the present calculation and (b) comparison of the present result with those from tDMRG calculations. The broadening factor is commonly $0.2t$. The periodic boundary condition is adopted in our calculation, whereas in the tDMRG calculation, the open boundary condition is adopted. The tDMRG results are reprinted from Ref. [20].

To better understand the nature of this lowest peak, we lift the restriction for J's mentioned above and change the parameter values rather freely. In Fig. 4, we provide an overview of the calculated spectra for U/t=10((a) and (c)), with the charge correlations ((b) and (d)). Here, the polarization of light is directed horizontally, and the charge correlation is defined to provide a doublon distribution around the holon at the origin. In (a) and (b), the parameters are set to $J_{\rm ex}$=$J_{\rm 3site}$=J and J is changed as listed. Hereafter, the artificial broadening γ for the spectra is $0.1t$ unless stated explicitly. Note that the value for the Hubbard model with U/t=10 is approximately $0.4t$. In (c) and (d), on the other hand, we show the results for $J_{\rm ex}$=J with $J_{\rm 3site}$=0. Because the detailed analyses are described later, we mention only the basic points here. Focusing on the region specified by the ovals in (a) and (c), we identify two (four) optically allowed states for the former (latter) cases, respectively. Note that, in (a) with J/t=0.4, the two peak energies are rather close to each other, and in (c) with J/t=0.4, the highest-energy peak is absorbed in the part above it. As a trend common to both the cases, we notice that the absorptions in these regions split off from the higher-energy part more clearly when we increase the J value. Regarding the lowest-energy optically allowed state, each state appears as a sharp peak. At a glance, this seems to indicate a DH bound state, although it is not fully compatible with the feature in the charge correlations. For instance, in those for J/t=0.4 (top panels in (b) and (d)), no meaningful feature indicates localization of the doublon at the expected sites ((±1, 0)). By contrast, when the J value is relatively large, we recognize a tendency for DH binding, for example, in (d) with J/t=2.0, although the degree of binding is somewhat imperfect when $J_{\rm 3site}$>0, as shown in (b) with J/t=2.0. We will discuss these features later.

Next, we investigate the features found for $J_{\rm 3site}$=0 more closely, focusing on the level structure in the low-energy region of the spectrum, as shown in Fig. 4(c). To simplify this situation, we draw the spectrum in this region for a larger J value, as shown in Fig. 5(a). The four states mentioned above, #1∼#4, appear more clearly and are separated from the higher-energy part. Figure 5(b) shows the energy differences between the corresponding peaks specified by the arrows in (a), as a function of $J_{\rm ex}/t$. As already mentioned, the interval between a peak in this part and the lowest-energy peak in the remaining higher absorption part depicted by the triangles or squares increases monotonically as the value of $J_{\rm ex}$ is increased. By contrast, the width of the lowest part remains almost constant as specified by the circles, the reason for which is explained later. Regarding the nature of the states, we show the charge density patterns in (c). For example, in the first state (#1), most of the weight is concentrated at the position (±1, 0) (site A defined in (d)), which is natural for a bound DH pair. The bright spot at (±3, ±4) is equivalent to this by translational symmetry. In addition, we find that the sites with significant weights are only B, C, and D in (d), except for the equivalent sites owing to the present symmetry. We refer to these states as "essential states" from here on.

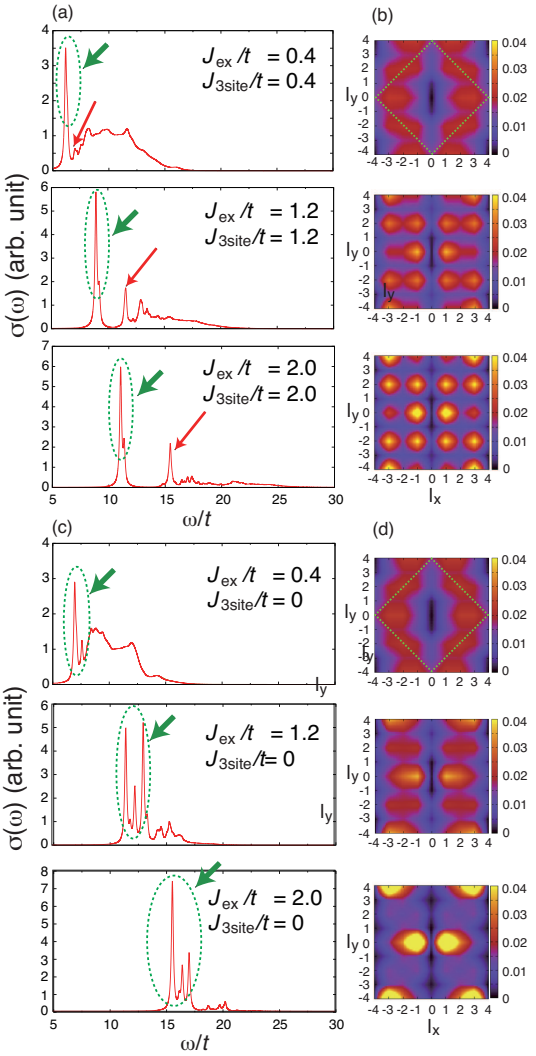

FIG. 4. Optical conductivities and charge patterns for U=$10t$. In the latter, the hole resides at the origin and the relative density distribution of the doublon is plotted with interpolation. In (a) and (b), $J_{\rm ex}$=$J_{\rm 3site}$=J, whereas in (c) and (d), $J_{\rm ex}$=J, but $J_{\rm 3site}$=0. In (b) and (d), the summed density inside the dashed area (cluster size) is normalized to unity.

As the mechanism providing such essential states, we propose the idea illustrated in Fig. 6. First, because we are concerned with the lowest optically excited states, we begin with a state having the least modification of the AF order in the ground state. This is "A" in the top-left panels both in (a) and (b). Here, "A" has two meanings, namely, the site where the hole resides and the state in which the spin arrangement is almost the same as that in the ground state. As is already mentioned in the introduction, the bare excitation energy is U+$3.5J_{\rm ex}$, counting

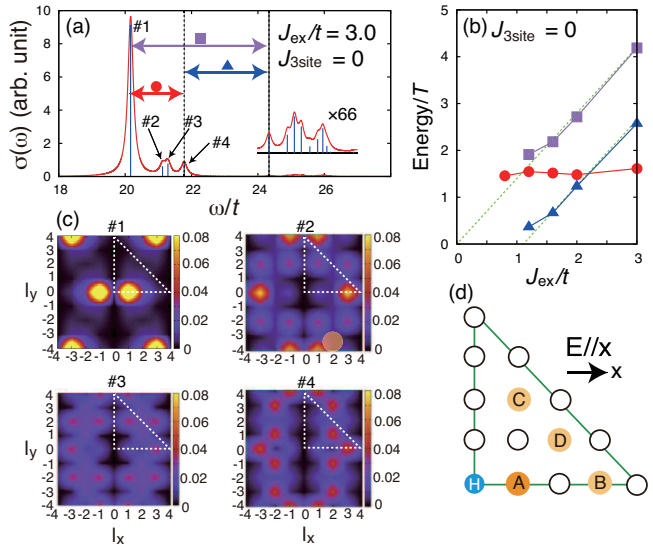

FIG. 5. Results in the absence of J_{3site}. (a) Optical conductivity for J_{ex}=3.0t, (b) J_{ex}-dependence of the energy intervals appearing in (a), (c) charge-distribution maps, and (d) a schematic showing A∼D states.

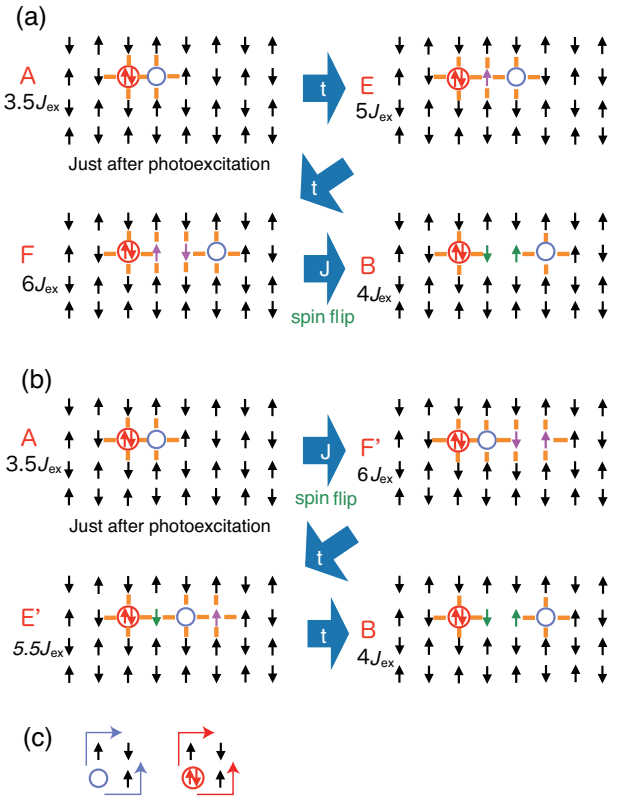

FIG. 6. Schematics showing the two processes corresponding to A→B transitions.

seven mismatches (orange bonds). From here on, we only refer to its magnetic part, for example, 3.5J_{ex}, apart from U.

First, we explain Process 1, which is illustrated in Fig. 6(a). If we consider the hole motion, the hole moves to site E via the transfer of the neighboring up spin. This state has an energy of 5J_{ex}. This up spin cannot flip by itself, because of the conservation of S_z, and flipping of this spin requires flipping of the surrounding spins, which requires further energy. When the hole moves further in the same direction, it reaches site F or state F, which corresponds to the energy of 6J_{ex}. At this site, two spins intervene along the path of the hole, and their flipping is possible. After such flipping, we obtain the B state (the bare energy is 4J_{ex}). Note that states F and B share the same hole site but have different spin configurations. We mostly mention the B state and call the corresponding site "B site". Lastly, there are two similar sites, which are the "C" and "D" mentioned above.

In contrast to Process 1, in which the hole movements occur before the spin flipping, Process 2 is characterized by the rule that the spin flip occurs before the carrier movement, as shown in (b). In this case, the intermediate states are denoted as E' and F'. When we exchange the initial and final states, the roles of the two processes are also exchanged, and both processes must be included for consistency.

Here, we actually evaluate how the AF order in the ground state is maintained in the lowest optically allowed states. For this purpose, we calculated the spin correlation function defined as $S(l) \equiv (1/N)\langle \sum_i \boldsymbol{S}_{i+l}\boldsymbol{S}_i \rangle$ for the excited states #1∼#4, which are shown in Fig. 7(a) together with that in the ground state [Fig. 7(b)]. The results demonstrate that the AF order is really maintained in all the excited states #1∼#4. These features are also consistent with the preceding interpretation based on the dynamical mean-field theory [17].

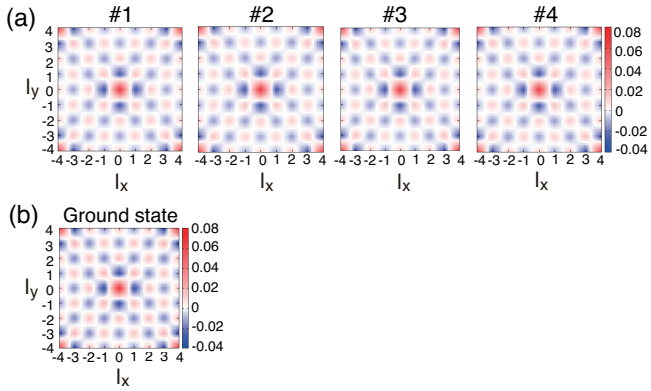

FIG. 7. Spin correlation function, $S(l)$, for J_{ex}/t=3.0 and J_{3site}=0. In (a), $S(l)$ is plotted for the lowest four states in Fig. 5(a). For comparison, $S(l)$ in the ground state is also shown in (b).

From here on, we focus on the level structure of the excited states #1∼#4. In Fig. 8(a), we plot the relative energies in this region by circles, changing the J_{ex} values. Note that each energy position of the second state

(#2), $e(2)$, is used as a reference. We use this selection because it is conjectured that the continuum part of the states starts from this position, and this conjecture is confirmed to be true later. As aforementioned, the spanned energy width, i. e., $e(4) - e(1)$, does not depend significantly on $J_{\rm ex}$, while the inner level distribution drastically changes. In particular, the lowest state departs from the other states, which suggests the formation of a single bound state in large clusters. We believe that this expectation is consistent with the aforementioned bare energies, namely, $3.5J_{\rm ex}$ for a single state (state A) and $4J_{\rm ex}$ for other BCD-like states. From here on, we name the latter as "low energy bulk states." In this scenario, we also expect that the upper three states will make a continuum in an infinite system. When we return to the present cluster, the energy spanned by the three higher states shrinks significantly with increasing $J_{\rm ex}$, which is consistent with the almost constant whole width because the lowest state splits off almost linearly with $J_{\rm ex}$. This shrinkage of the higher part is directly related to the matrix elements of the processes in Fig. 6, dominated by the factor of $t^2/J_{\rm ex}$, which is explained in detail later.

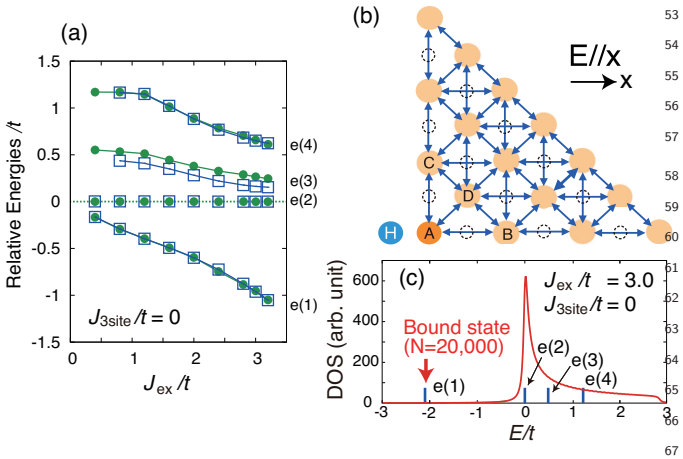

FIG. 8. In (a), $J_{\rm ex}$-dependent low-lying energy levels obtained without $J_{\rm 3site}$, for N=32. The squares (circles) show the energies calculated using the effective model I (II). In (b), a schematic for the effective model II is illustrated, and, in (c), the density of states (DOS) for $J_{\rm ex}/t$=3.0, and N=20,000 is plotted with the energy levels for the case with the same J_{ex}/T and N=32 (vertical bars). Note that both are calculated by the effective model II. The single bound state for N=20,000 is located very close to $e(1)$. The energies in (a) and (c) are measured from $e(2)$ for N=32.

III. EFFECTIVE MODEL II AND THE RESULTS BASED ON IT

To substantiate this scenario, we propose an effective model (effective model II), which includes only the A and low energy bulk states, as shown in Fig. 8(b). Here, we start the procedure by assuming that the $J_{\rm ex}$ value is sufficiently large compared to t and apply a third-order perturbational analysis. Because we explain the details in Appendix B, we add only one point here. The effective transfer is proportional to $(t^2J_{\rm ex})/J^2{=}t^2/J_{\rm ex}$, particularly for a large $J_{\rm ex}$, in the third-order perturbational sense as illustrated in Figs. 6(a) and (b). This explains the shrinking of the bandwidth of the possible continuum part for a large $J_{\rm ex}$, as previously mentioned. The circles in Fig. 8(a) show the resultant curves. Although there remains a slight difference, we judge that the reproduction is fairly good. We then calculate the density of states per site (DOS) for $J_{\rm ex}{=}3.0t$ and N=20,000, with the energy levels for N=32, as shown in Fig. 8(c). The obtained DOS shows a sharp structure at the lower edge of the continuum. This is related to the enhanced effective transfers along the diagonal direction, which provides such a one-dimensional feature. In more detail, we expect two paths for the H or D movement in the diagonal direction, which are the path going around the upper side and that around the lower side (see Fig. 6(c)). They can overlap with each other coherently, leading to the enhancement. With respect to the overall bandwidth, it is much larger than the spanned energy in the case of N=32. A close analysis of the size dependency indicates that there is a jump in the bandwidth when the size changes from N=32 to the next size in this scheme, N=72. We emphasize that the bandwidth in (c) has almost converged, because of the large size used.

Regarding our central concern, the bound state, we recognize its existence for any positive value of $J_{\rm ex}$. In Fig. 9, we plot the energy position measured from the lower edge of the continuum. Note that the values (squares) are extrapolated to the infinite size. Although there is a slight drop in the absolute value from that for N=32, particularly for smaller $J_{\rm ex}$ values, we observe that the binding energy is always finite, except for a very small $J_{\rm ex}$ region. Charge patterns of the bound states are also worth close observation. In the same figure, we show them for four typical $J_{\rm ex}$ values. In these maps, we only show the non-equivalent quadrant, in which the D density around the H at the origin is plotted. Note that the density is normalized in this quadrant. The largest $J_{\rm ex}$ case, namely, that for $J_{\rm ex}{=}3.2t$, shows the most localized pattern, whereas those for the smaller $J_{\rm ex}$ cases show more delocalized patterns. A special remark is made for its extended nature along the diagonal line, which is attributable to the aforementioned enhanced hopping matrix elements along the diagonal direction.

Finally, we discuss the effects of the $J_{\rm 3site}$ on DH-binding. Part of its effect is the effective hopping to next n. n. sites without disturbing the AF order in the background. Therefore, we expect an effect toward less binding provided by this term and confirm it in the following. First, we check whether the term of $J_{\rm 3site}$ is appropriately incorporated into the effective model II, and show the level structure for N=32, with the selection of $J_{\rm 3site}{=}J_{\rm ex}{=}J$. In Fig. 10(a), we show the result using

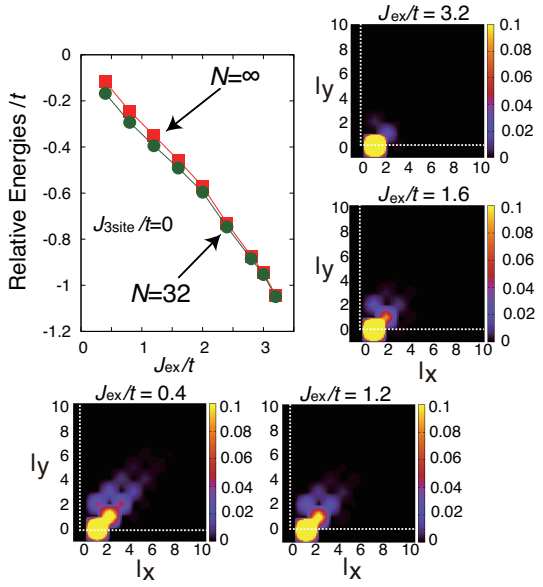

FIG. 9. Relative energies of the bound state measured from the lower edge of the continuum for various $J_{\rm ex}$ values and corresponding charge patterns. Note that $J_{\rm 3site}$=0.

triangles, which are compared with those obtained without $J_{\rm 3site}$ (circles). As an overall feature, the original four states split into three parts: one state with the highest energy, one state staying around the original energies, and two almost degenerate states at low energies. Compared with the spectra in Fig. 4(a), the lowest two states are attributable to those specified by thick arrows in Fig. 4(a) and the middle state to that specified by thin arrows. An example is shown in Fig. 10(b), using the case of J=3.0t. Here, the obtained energy levels (vertical lines), with the energy shift of the latter by (-2.3)t, is compared with the spectral peaks. This energy shift is interpreted to be due to the imperfect inclusion of fluctuation in the effective model II. Assuming this energy shift, we notice a satisfying agreement except for the highest-energy region, in which the electronic states are difficult to treat by the effective model II. Furthermore, aiming at more accuracy, we compare the two intervals, namely, that between the lowest state and the third state (middle state) in the effective model II and that in the effective model I, i. e., the interval between the energies specified by the two arrows in Fig. 4(a). We consequently find that there is a slight difference, particularly in the small J region, as shown in Fig. 12 in Appendix C. In particular, in the effective model II, the effect of $J_{\rm 3site}$ is somewhat exaggerated in the smaller J region. Because we prepared the effective model II without the $J_{\rm 3site}$ term, we now judge that another adjustment is required in the presence of $J_{\rm 3site}$ and modify its value so as to reproduce the intervals found for the effective model I.

The $J_{\rm 3site}$ values thus determined for each $J_{\rm ex}$=J are plotted by squares in the $J_{\rm ex}$-$J_{\rm 3site}$ diagram (Fig. 10(c)). The circles correspond to the boundary between a bound case and an unbound case, which is accurately determined by the extrapolation to N=∞. Focusing on the squares, we observe that the larger J cases are contained in the unbound region, whereas smaller J cases fall into the bound cases, although direct analyses of energy levels indicate that all the binding energies are less than 0.1t. In Figs. 10(d) and (e), we show the details of such a bound state, particularly in the case of $J_{\rm ex}$=0.4t, which corresponds to the case of the Hubbard model with U=10t. Local density of states (LDOS) in (d), which is defined as the DOS projected onto the A site and approximates the optical conductivity, has a sharper structure at the lowest energy than the DOS, originating from its bound nature. The charge pattern in (e) also indicates the bound nature, which is basically the same as that appearing in the corresponding density map in Fig. 9, although the former is more extended.

In Fig. 11, we show the charge correlations for four cases along the line of $J_{\rm ex}$=0.4t, to understand the nature of the states more deeply. The top-left map ($J_{\rm 3site}$=0) is essentially the same as that appearing as the bottom-left map in Fig. 9, and the top right ($J_{\rm 3site}$=0.07t) is the same as that shown in Fig. 10(e). The bottom-left map ($J_{\rm 3site}$=0.40t) corresponds to the result before the adjustment of $J_{\rm 3site}$, which also indicates a binding nature, although it is much more widespread than the previous ones. Finally, the bottom-right map ($J_{\rm 3site}$=0.60t) is for the case which is inside the unbound region but still close to the phase boundary. As expected, the pattern is two-dimensionally spread.

IV. CONCLUSION AND FUTURE PERSPECTIVE

We examined the photoexcited states of the 2D Mott insulators, focusing on the case of the Hubbard model with U=10t. The optical conductivity obtained using the effective model I with N=32 exhibited a sharp peak structure at the lower edge. To clarify the nature of this structure, we proposed the effective model II and found that in the absence of $J_{\rm 3site}$, a single DH pair forms a bound state irrespective of the $J_{\rm ex}$ value. In contrast, when we introduced $J_{\rm 3site}$, there was a tendency for much less binding. In particular, the pair is bound, only for $J_{\rm 3site} \lesssim J_{\rm ex}$. In the present scheme based on the effective model II, the Hubbard case with U=10t falls into a bound case, maintaining the sharp peak at the lower edge as observed in the calculated spectrum by the effective model I, whereas the binding energy is very small. In this respect, however, we think that the accurate judgment for the binding is still difficult because of the limited precision of the present effective models. What we can confidently state is that the case is close to the bound-unbound boundary.

As discussed, the $J_{\rm 3site}$ term greatly enhances the effective itineracy, which yields a widespread whole band and a significant suppression in the DH binding energy. Such

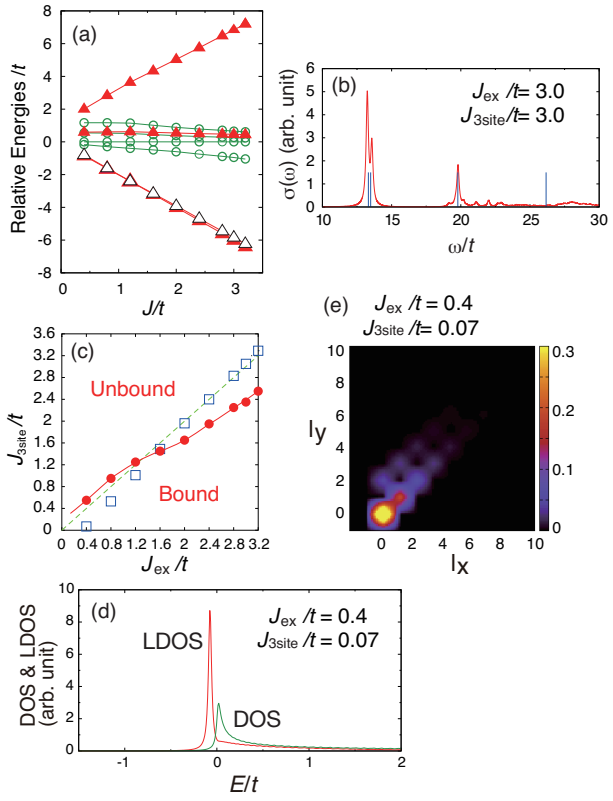

FIG. 10. Results for $J_{3\mathrm{site}}>0$. (a) Energy levels determined by the effective model II for N=32, with J_{ex}=$J_{3\mathrm{site}}$=J (triangles), and J_{ex}=J and $J_{3\mathrm{site}}$=0 (circles), (b) optical conductivity spectrum from the effective model I (curve) and the energy levels from the effective model II (vertical lines), both obtained with N=32 and J_{ex}=$J_{3\mathrm{site}}$=3.0t, (c) phase diagram, where the two variables, $J_{3\mathrm{site}}$ and J_{ex}, are selected independently, (d) DOS and local DOS (LDOS), and (e) a charge pattern, for J_{ex}/T=0.4 and $J_{3\mathrm{site}}/t$=0.07. In (a), the triangles and circles correspond to the cases with and without $J_{3\mathrm{site}}$, respectively. The energy in (a) is measured from $e(2)$ for the case of N=32 and $J_{3\mathrm{site}}$=0, and that in (d) is measured from the lower edge of the continuum. In (b), the energies of the levels are shifted by (-2.3)t to make them match the peaks of $\sigma(\omega)$.

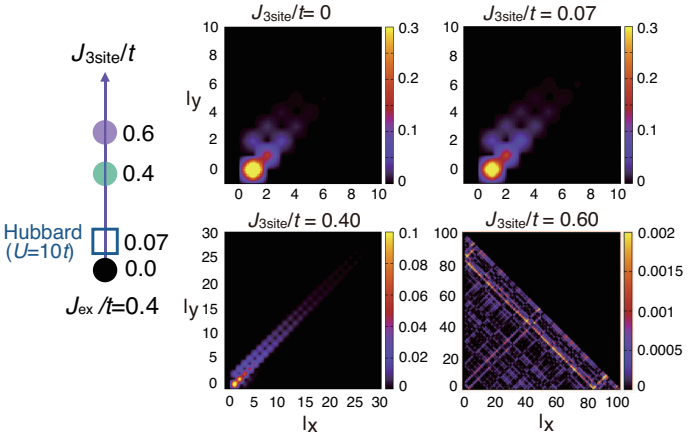

FIG. 11. Charge correlations for the cases corresponding to the points specified on the left side. J_{ex} is fixed at 0.4t. The case of $J_{3\mathrm{site}}$=0.07t (square) corresponds to the case of the Hubbard model, with U=10t.

effects manifest itself as a drastic change in the spectra, as demonstrated by the comparison between Figs. 4(a) and (c). Because the effect of $J_{3\mathrm{site}}$ cannot be neglected when we discuss the photoexcited states of the Hubbard model, we think that such a strong suppression of the DH binding is characteristic of this system.

We also address the relationship with the observations in actual materials. The optical conductivity spectra observed in various copper oxides commonly show enhancement at the lower edge [30–36]. We assign the sharp peak originating from the DH binding to the observed structures. In particular, the theoretically found nature of the weakly bound pair is consistent with the spectral feature of the observation, namely, the enhancement that is not isolated from the continuum part above it. Next, since the situation of the Hubbard model with U=10t is subtle as mentioned above, there still remains the possibility of no DH binding. Even in this case, it is expected that a sharp structure will remain even if we lose the DH binding because of the property of the DOS. Based on such interpretations, we basically think that the present results are consistent with the observed optical conductivities.

We also state two effects not considered in our analyses. The corresponding part of the spectrum is much broader in the observation. We suppose that possible fluctuations originating from the remaining effects, such as electron-phonon interactions, might broaden the peak, leading to a width (FWHM) around 0.2∼0.3 eV [36]. Another point is the possibility that Coulombic interaction working between n. n. sites (the so-called V term in the extended Hubbard model) enhances this peak structure. We suppose that this effect is subsidiary because a large parameter value for V, 5∼6 t at least, is required to produce a bound state [37]. Therefore, we believe that the magnetic origin of the sharp structure is essential, and that this finding will shed a new light on the low-energy properties of photodoped carriers in 2D Mott insulators.

ACKNOWLEDGMENTS

The authors acknowledge Dr. K. Shinjo, Prof. T. Tohyama, and Prof. A. Takahashi for fruitful discussions. This work was supported by the JST CREST in Japan (Grant No. JPMJCR1661). K. I. was supported by a Grant-in-Aid for Scientific Research from JSPS in Japan (Grant No. JP17K05509). H. O. was supported by a Grant-in-Aid for Scientific Research from JSPS in Japan (Grant No. JP21H04988). The computations were performed at the Research Center for Computational Science, Okazaki, Japan, and at RCNP and CMC of Osaka University, Osaka, Japan.

Appendix A: Derivation of the effective model I

We briefly describe the derivation of the effective model I, which is based on the established procedure of a t/U-expansion. This procedure is a unitary transformation that aims to eliminate the matrix elements connecting states for different DH pair numbers [23–25]. The original procedure was applied to the ground state in the Hubbard model. Here, we apply it to photoexcited states, particularly with a single DH pair to create an effective model. The same effective model was derived using a slightly different formulation [21, 22]. However, the procedure of the unitary transformation is more systematic, in the sense that the current operator is also transformed at the same time, and an explicit description is worth mentioning.

First, the unitary transformation is formally written for the effective model I, $H^{\rm eff}$, as

$$H^{(\rm eff)} \equiv e^{iS} H e^{-iS} \ , \tag{A1}$$

where H is the original Hubbard model and $S \equiv S^{[1]} + S^{[2]} + ...$ is the generator of the transformation, with $S^{[k]}$ being of the kth-order of t/U. As aforementioned, we select $S^{[k]}$'s to eliminate the matrix elements of H between the two states belonging to different subspaces. Note that we define subspaces such that each has a fixed DH pair number. After some derivation, we find

$$iS^{[1]} = U^{-1}(T_1 - T_{-1}) \tag{A2}$$

$$iS^{[2]} = U^{-2}[T_1 + T_{-1}, T_0] \ , \tag{A3}$$

where

$$T_1 \equiv \sum_{m\geq 0} P_{m+1} T P_m \ , \tag{A4}$$

$$T_{-1} \equiv \sum_{m\geq 1} P_{m-1} T P_m \ , \tag{A5}$$

$$T_0 \equiv \sum_{m\geq 0} P_m T P_m \ , \tag{A6}$$

with T and P_m being the kinetic part of H and the projection operator into a subspace of m DH pairs. Using this selection, the resultant effective hamiltonian can be written as

$$H^{(\rm eff)} = V_c + T_0 + U^{-1}[T_1, T_{-1}] + O(U^{-2}) \ , \tag{A7}$$

where V_c is the site-diagonal term of H, that is, the U-term. Using the same transformation, we obtain an effective expression for the current operator as

$$J^{(\rm eff)} = J + U^{-1}[T_1 - T_{-1}, J] + O(U^{-2}) \ . \tag{A8}$$

Furthermore, we decompose J as $J{=}J_1{+}J_{-1}{+}J_0$, where

$$J_1 \equiv \sum_{m\geq 0} P_{m+1} J P_m \ , \tag{A9}$$

$$J_{-1} \equiv \sum_{m\geq 1} P_{m-1} J P_m \ , \tag{A10}$$

$$J_0 \equiv \sum_{m\geq 0} P_m J P_m \ , \tag{A11}$$

and we find a simpler form as

$$J_1^{(\rm eff)} = J_1 + U^{-1}[T_1, J_0] + O(U^{-2}) \ . \tag{A12}$$

Expanding the above $H^{(\rm eff)}$, we define its four components as

$$H^{(\rm eff)} = H_1 + H_2 + H_3 + H_4 \ , \tag{A13}$$

$$H_1 \equiv V_c + T_0 \ , \tag{A14}$$

$$H_2 + H_3 \equiv -U^{-1} T_{-1} T_1 \ , \tag{A15}$$

$$H_4 \equiv U^{-1} T_1 T_{-1} \ . \tag{A16}$$

Note that, at this stage, H_2 and H_3 are not yet separated. According to Ref. [21], they are separated into a term in which two nearest-neighboring spin sites are involved, and a term in which three consecutive sites, with a D or H site located at the end, are involved (refer to Fig. 1). The former, which we denote as H_2, is the spin-exchange term expressed as $H_2 = J_{\rm ex} \sum_{ll'} \boldsymbol{S}_l \boldsymbol{S}_{l'}$, where $\boldsymbol{S}_l$ is the usual spin operator at site l. Note that l is a 2D site index. In contrast, the latter term (H_3) corresponds to the transfer of a D or an H by two sites, known as the three-site term. The explicit form is

$$H_3 = -\frac{1}{4} J_{\rm 3site} \{ \sum_{<e,k,l>,\sigma,\sigma'}^{k,l\in\bar{S},e\in\bar{E}} C^\dagger_{e\sigma} C_{k\sigma} C^\dagger_{k\sigma'} C_{l\sigma'} + \sum_{<d,l,k>,\sigma,\sigma'}^{k,l\in\bar{S},d\in\bar{D}} C^\dagger_{l\sigma} C_{d\sigma} C^\dagger_{k\sigma'} C_{l\sigma'} \} \ . \tag{A17}$$

Here, $< i,j,k >$ are three different sites, where both the site pairs $< i,j >$ and $< k,l >$ are nearest neighbors, and $\bar{S}$, $\bar{E}$, and $\bar{D}$ denote the sets of sites, consisting of singly occupied sites, empty sites, and doubly occupied sites, respectively. Note that both $J_{\rm ex}$ and $J_{\rm 3site}$ are $4T^2/U$ when we follow the Hubbard model perfectly, although we lift this restriction and change it freely, as mentioned in the main text. In contrast, the last term, H_4, is associated with the processes in which the states with no DH pair are intermediate states. We emphasize that this term is irrelevant in the present calculation of the photoexcited states. Actually, the processes are forbidden, because the photoexcited states have odd parity with respect to the charge conjugation (CC), whereas all the states with no DH pair have even CC parity.

Appendix B: Derivation of the effective model II

In this section, we derive the effective model II, particularly for the case of $J_{\rm ex} = J$ and $J_{\rm 3site}{=}0$. The effect of $J_{\rm 3site}$ is included later straightforwardly. We follow the procedure used in the derivation of the effective model I, although the basic meanings of the states are largely different. First, we define the following Hamiltonian;

$$h \equiv \hat{T} + \hat{V} \ , \tag{B1}$$

where

$$\hat{T} \equiv \sum_{i\in S_{\rm ABCD}, j\in S_{\rm E}} \{t^{(1)}_{ji}|j><i| + h.c.\} + \sum_{i\in S_{\rm ABCD}, j\in S_{\rm F}} \{t^{(2)}_{ji}|j><i| + h.c.\} + \sum_{i\in S_{\rm E}, j\in S_{\rm F}} \{t^{(3)}_{ji}|j><i| + h.c.\} \ , \quad \text{(B2)}$$

and

$$\hat{V} \equiv \sum_i e_s(i)|i><i| \ . \quad \text{(B3)}$$

Here, $|i>$ is limited to (A-F)-like states, and $S_{\rm ABCD}$ and S_μ (μ=E, F) are the subspaces to which (A-D)-like states and μ-like states, respectively, belong. $e_s(i)$ are their bare state energies, e_s(A)=3.5J, e_s(B$\sim$D)=4J, $e_s(\mu)$=5J or 5.5J for μ=E, and $e_s(\mu)$= 6J or 6.5J for μ=F. The two choices of the $e_s(\mu)$ for μ=E, F are summarized as follows. First, we emphasize that each E- or F-like state is associated with a certain (A-D)-like state. This fact is almost trivial because the F-like state shares a holon site with one of the latter states. Regarding the E-like state, we focus on the four surrounding spins around the holon and observe that one of the spins is different from that of the others. For example, for the E-like state in Fig. 6(a), only one up spin exists on the left side. We then define the E-like state as being associated with the (A-D)-like state that has the holon at this position. After simple arithmetic, we can easily find that e_s(E)=5J (5.5J) for the E-like states associated with the A state (low energy bulk states). Similarly, we also find that e_s(F)=6J (6.5J) for the F-like states associated with the A state (low energy bulk states).

From this model, we derive the effective model II by eliminating the E- and F-like states. To do so, we apply a third-order perturbational analysis. Namely, we divide the entire Hilbert space into two subspaces: the subspace of the (A-D)-like states and those of the E- and F-like states, and use a unitary transformation that dismisses the interactions between the former and latter subspaces, as is done in deriving the effective model I. The difficulty is that the diagonal energies, $e_s(i)$, are not homogeneous within each subspace. To avoid this, we redefine the Hamiltonian as follows.

$$h = V_0 + V_1 + \tilde{T}_0 + \tilde{T}_1 + \tilde{T}_{-1} \ . \quad \text{(B4)}$$

The first two terms confine the states within each subspace, as

$$V_0 = \sum_{i\in S_E\cup S_F} (2J)|i><i| \quad \text{(B5)}$$

$$V_1 = (-0.5J)|A><A| + \sum_{i\in S_E\cup S_F} (e_s(i)-6J)|i><i| \quad \text{(B6)}$$

$$\tilde{T}_0 = \sum_{i\in S_{\rm E}, j\in S_{\rm F}} \{t^{(3)}_{ji}|j><i| + h.c.\} \ . \quad \text{(B7)}$$

Note that we set a reference energy for each subspace, which is 4J and 6J for the ABCD subspace and the EF subspace, respectively, and that the difference between the two reference energies, that is, 2J, appears in Eq. B5. On the other hand, the last two terms provide the transitions between the two subspaces;

$$\tilde{T}_1 \equiv \sum_{i\in S_{\rm ABCD}, j\in S_{\rm E},} t^{(1)}_{ij}|j><i| + \sum_{i\in S_{\rm ABCD}, j\in S_{\rm F},} t^{(2)}_{ji}|j><i| \ , \quad \text{(B8)}$$

and

$$\tilde{T}_{-1} \equiv \sum_{i\in S_{\rm ABCD}, j\in S_{\rm E},} t^{(1)}_{ij}|i><j| + \sum_{i\in S_{\rm ABCD}, j\in S_{\rm F},} t^{(2)}_{ji}|i><j| \ . \quad \text{(B9)}$$

We emphasize that the "transfer" energies, $t^{(1)}_{ij}$ and $t^{(3)}_{ij}$ are proportional to t, while $t^{(2)}_{ij}$ to J. We omit actual expressions of them, because they are complicated due to the introduced spatial symmetries and the definitions of the basis set.

We apply a unitary transformation to this model. The transformation is defined as an expansion, as was done in constructing the effective model I. In this case, $t/(2J)$ is the expansion parameter and we use the property that $[V_0, T_m] = m(2J)T_m$. Consequently, the V_0 term plays the role of the Hubbard U term, and the transformation is expressed as follows;

$$h_{eff} \equiv e^{is} h e^{-is} \ , \quad \text{(B10)}$$

where $s \equiv s^{[1]} + s^{[2]} + ...$ with each $s^{[n]}$ being the nth-order of $t/(2J)$, and the following first three terms are sufficient for the present purpose;

$$is^{[1]} = (2J)^{-1}(\tilde{T}_1 - \tilde{T}_{-1}) \quad \text{(B11)}$$

$$is^{[2]} = (2J)^{-2}[\tilde{T}_1 + \tilde{T}_{-1}, \tilde{T}_0] \quad \text{(B12)}$$

$$is^{[3]} = (2J)^{-3}\Big\{ [[\tilde{T}_1 - \tilde{T}_{-1}, \tilde{T}_0], \tilde{T}_0] + \frac{1}{4}[[\tilde{T}_1, \tilde{T}_0], \tilde{T}_1] - \frac{1}{4}[[\tilde{T}_{-1}, \tilde{T}_0], \tilde{T}_{-1}] + \frac{2}{3}[\tilde{T}_1 + \tilde{T}_{-1}, [\tilde{T}_1, \tilde{T}_{-1}]] \Big\} \ . \quad \text{(B13)}$$

The resultant effective Hamiltonian of the third order, $h^{(3)}_{eff}$, which is defined as $h^{(3)}_{eff} \equiv \exp(is^{(3)}) h \exp(-is^{(3)})$,

using the definition, $s^{(k)} \equiv \sum_{i=1}^{k} s^{[k]}$, is expressed as

$$h_{eff}^{(3)} = \tilde{T}_0 + V_0 + V_1 + \frac{1}{2J}[\tilde{T}_1, \tilde{T}_{-1}] + \left(\frac{1}{2J}\right)^2 \Big\{ \tilde{T}_1(\tilde{T}_0 + V_1)\tilde{T}_{-1} + \tilde{T}_{-1}(\tilde{T}_0 + V_1)\tilde{T}_1 - \frac{1}{2}\tilde{T}_1\tilde{T}_{-1}(\tilde{T}_0 + V_1) - \frac{1}{2}\tilde{T}_{-1}\tilde{T}_1(\tilde{T}_0 + V_1) - \frac{1}{2}(\tilde{T}_0 + V_1)\tilde{T}_1\tilde{T}_{-1} - \frac{1}{2}(\tilde{T}_0 + V_1)\tilde{T}_{-1}\tilde{T}_1 \Big\} + O((2J)^{-3}) \ . \quad \text{(B14)}$$

As expected, the Hamiltonian is closed within each subspace. In particular, we have a special interest in the ABCD subspace. In this case, the effective transfers between the different constituent states are derived from one of the third-order terms, that is, that of $(1/2J)^2 T_{-1} T_0 T_1$ in Eq. B14. Regarding the other terms, the first two terms, namely, $\tilde{T}_0$ and V_0, are irrelevant in the ABCD subspace, and the third term, V_1, gives the energy lowering of $0.5J$ for the A state in the same subspace. The fourth term, that with the prefactor of $1/(2J)$, corresponds to the modification of the diagonal energy of each state. Returning to the third-order terms (those with the prefactor of $1/(2J)^2$), we have the terms including $\tilde{T}_1\tilde{T}_{-1}$, with subspace-diagonal terms as additional factors. These terms do not contribute at all. Actually, the operation of $\tilde{T}_{-1}$ does not change the present optically active states down to the ground states with no HD pair, because the latter states have the different CC symmetry. In contrast, the terms including $\tilde{T}_{-1}\tilde{T}_1$ provide finite contributions, which are corrections to the state-diagonal energies.

Our basic strategy for calculating large systems while keeping quantitative reliance is to reproduce the behaviors in Fig. 8(a) (green circles) with a model as simple as possible. For this purpose, first, we neglect most of the state-diagonal corrections. Instead, we allow a correction to the difference between the diagonal energy of A state and the other states ("BCD"-like states). Furthermore, we modify the effective transfers by scaling all of them with a single parameter, which adjustment is essential when applying this model to a small $J_{\rm ex}$. By this scaling, we can also include the effect of spin fluctuation inherent in the AF background, which reduces the absolute values of the effective transfer energies. As a whole, we have the two adjustment parameters for diagonal energies and transfer energies. Finally, we comment on the selection of V_0. In the present formulation, we set the "representative" energy difference of the two subspaces at $2J$, which is not a unique selection. If we select another value, we obtain a different expansion although the complete solution obtained after summing up the infinite series should be identical. This implies that at the level of $h_{eff}^{(3)}$, the results depend on this selection, and we, therefore, select the value to reduce the higher-order terms as much as possible, that is, the selection of the representative energy difference as the average of the energy differences.

Appendix C: Detailed results from the effective model II in the presence of $J_{\rm 3site}$

In Fig. 12, we show the $J_{\rm ex}$-dependence of the concerned energy interval for the three cases. The first case corresponds to the result obtained by the effective model I, which is shown by the triangles. The second one corresponds to the "raw" result obtained by the effective model II with $J_{\rm ex}$=$J_{\rm 3site}$=J (circles). There is a discrepancy between these values, particularly in the weak $J_{\rm ex}$ region. Consequently, we adjust the $J_{\rm 3site}$ value for each $J_{\rm ex}$, to reproduce the data from the effective model I, and obtain the values represented by the squares.

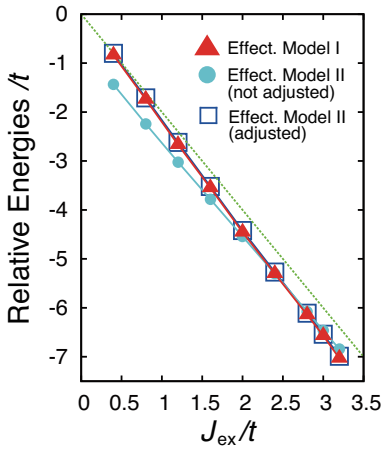

FIG. 12. $J_{\rm ex}$-dependence of the relative energies. Energy intervals of the first and third peaks obtained by the effective model II with $J_{\rm 3site}$ >0 are plotted as circles and squares. Here, the circles show the data without any adjustment for $J_{\rm 3site}$, that is, for $J_{\rm 3site}$=$J_{\rm ex}$, while the squares are obtained with adjustment. The results from the effective model I are specified by triangles.

[1] M. Imada, A. Fujimori, and Y. Tokura, Rev. Mod. Phys. **70**, 1039 (1998).
[2] E. Dagotto, Rev. Mod. Phys. **66**, 763 (1994).
[3] R. Strack and D. Vollhardt, Phys. Rev. B **46**, 13852 (1992).
[4] W. Metzner, P. Schmit, and D. Vollhardt, Phys. Rev. B **45**, 2237 (1992).
[5] G. Sangiovanni, A. Toschi, E. Koch, K. Held, M. Capone, C. Castellani, O. Gunnarsson, S.-K. Mo, J. W. Allen, H.-D. Kim, A. Sekiyama, A. Yamasaki, S. Suga, and P.

Metcalf, Phys. Rev. B **73**, 205121 (2006).
[6] D. N. Sheng, Y. C. Chen, and Z. Y. Weng, Phys. Rev. Lett. **77**, 5102 (1996).
[7] Z. Zhu, H.-C. Jiang, Y. Qi, C. Tian, and Z.-Y. Weng, Sci. Rep. **3**, 2586 (2013).
[8] E. Jeckelmann, F. Gebhard and F. H. L. Essler, Phys. Rev. Lett. **85**, 3910 (2000).
[9] H. Kishida, H. Matsuzaki, H. Okamoto, T. Manabe, M. Yamashita, Y. Taguchi, and Y. Tokura, Nature (London) **405**, 929 (2000).
[10] Y. Mizuno, K. Tsutsui, T. Tohyama, and S. Maekawa, Phys. Rev. B **62**, R4769 (2000).
[11] H. Kishida, M. Ono, K. Miura, H. Okamoto, M. Izumi, T. Manako, M. Kawasaki, Y. Taguchi, Y. Tokura, T. Tohyama,
[12] M. Ono, K. Miura, A. Maeda, H. Matsuzaki, H. Kishida, Y. Taguchi, Y. Tokura, M. Yamashita, and H. Okamoto, Phys. Rev. B **70**, 085101 (2004). K. Tsutsui, and S. Maekawa, Phys. Rev. Lett. **87**, 177401 (2001).
[13] F. H. L. Essler, F. Gebhard, and E. Jeckelmann, Phys. Rev. B **64**, 125119 (2001).
[14] E. Dagotto, A. Moreo, F. Ortolani, J. Riera, and D. J. Scalapino, Phys. Rev. B **45**, 10107 (1992).
[15] T. Tohyama, Y. Inoue, K. Tsutsui, and S. Maekawa, Phys. Rev. B **72**, 045113 (2005).
[16] H. Nakano, Y. Takahashi, and M. Imada, J. Phys. Soc. Jpn. **76**, 034705 (2007).
[17] C. Taranto, G. Sangiovanni, K. Held, M. Capone, A. Georges, and A. Toschi, Phys. Rev. B **85**, 085124 (2012).
[18] E. W. Huang, R. Sheppard, B. Moritz, and T. P. Devereaux, Science **366**, 987 (2019).
[19] X.-J. Han, Y. Liu, Z.-Y. Liu, X. Li, J. Chen, H.-J. Liao, Z.-Y. Xie, B. Normand, and T. Xiang, New J. Phys. **18**, 103004 (2016).
[20] K. Shinjo, Y. Tamaki, S. Sota, and T. Tohyama, Phys. Rev. B **104**, 205123 (2021).
[21] A. Takahashi, S. Yoshikawa, and M. Aihara, Phys. Rev. B **65**, 085103 (2002).
[22] H. Itoh, A. Takahashi, M. Aihara, Phys. Rev. B **73**, 075110 (2006).
[23] A. B. Harris and R. V. Lange, Phys. Rev. **157**, 295 (1967).
[24] A. H. MacDonald, S. M. Girvin, and D. Yoshioka, Phys. Rev. B **37**, 9753 (1988).
[25] A. L. Chernyshev, D. Galanakis, P. Phillips, A. V. Rpzhkov, and A.-M, S. Tremblay, Phys. Rev. B **70**, 235111 (2004).
[26] Y. Saad, "Iterative Methods for Sparse Linear Systems," second edition, Society for Industrial and Applied Mathematics, 2013.
[27] E. R. Gagliano and C. A. Balseiro, Phys. Rev. Lett. **59**, 2999 (1987).
[28] M. Hirayama, Y. Yamaji, T. Misawa, and M. Imada, Phys. Rev. B **98**, 134501 (2018).
[29] The effective transfers in the effective model II are proportional to the product of the two consecutive bare transfers, which take opposite signs owing to the effect of phase strings in the case of the perfectly ordered AF. Thus, the effective transfers always have a negative sign in the absence of fluctuation. On the other hand, a finite amount of spin fluctuations is expected to reduce the absolute values of the effective transfers.
[30] Y. Tokura, S. Koshihara, T. Arima, H. Takagi, S. Ishibashi, T. Ido, and S. Uchida, Phys. Rev. B **41**, 11657 (1990).
[31] S. L. Cooper, G. A. Thomas, A. J. Millis, P. E. Sulewski, J. Orenstein, D. H. Rapkine, S-W. Cheong, and P. L. Trevor, Phys. Rev. B **42**, 10785 (1990).
[32] S. Uchida, T. Ido, H. Takagi, T. Arima, Y. Tokura, and S. Tajima, Phys. Rev. B **43**, 7942 (1991).
[33] A. V. Chubukov and D. M. Frenkel, Phys. Rev. B **52**, 9760 (1995).
[34] H. Kishida, M. Ono, A. Sawa, M. Kawasaki, Y. Tokura, and H. Okamoto, Phys. Rev. B **68**, 075101 (2003).
[35] A. Maeda, M. Ono, H. Kishida,T. Manako, A. Sawa, M. Kawasaki, Y. Tokura, and H. Okamoto, Phys. Rev. B **70**, 1 (2004).
[36] T. Terashige, T. Ono, T. Miyamoto, T. Morimoto, H. Yamakawa, N. Kida, T. Ito, T. Sasagawa, T. Tohyama, and H. Okamoto, Sci. Adv. **5**, 2187 (2019).
[37] K. Iwano, *unpublished.*